Apoptosis-inducing antitumor efficacy of hexokinase II inhibitor in hepatocellular carcinoma

Won Kim,[1] Jung-Hwan Yoon,[1] Jae-Min Jeong,[2] Gi-Jeong Cheon,[3] Tae-Sup Lee,[3] Jong-In Yang,[1] Su-Cheol Park,[1] and Hyo-Suk Lee[1]

[1]Department of Internal Medicine and Liver Research Institute and [2]Department of Nuclear Medicine, Seoul National University College of Medicine; [3]Department of Nuclear Medicine, Korea Institute of Radiological and Medical Sciences, Seoul, Korea

Abstract

Hypoxia stimulates hepatocellular carcinoma (HCC) cell growth via hexokinase (HK) II induction, and alternatively, HK II inhibition induces apoptosis by activating mitochondrial signaling. This study was to investigate whether the induction of HK II by hypoxia is associated with enhanced mitochondrial stability and to confirm the apoptosis-inducing efficacy of HK II inhibitor in an *in vivo* model of HCC. Mitochondrial stability was examined by treating isolated mitochondria with deoxycholate, a permeability-enhancing agent. Alteration of permeability transition pore complex composition was analyzed by immunoprecipitation and immunoblotting. An *in vivo* model of HCC was established in C3H mice i.d. implanted with MH134 cells. The antitumor efficacy of i.p. given 3-bromopyruvate (3-BrPA), a HK II inhibitor, was evaluated by measuring tumor volumes and quantifying apoptosis using terminal deoxynucleotidyl transferase–mediated dUTP nick end labeling staining and ^{99m}Tc-hydrazinonicotinamide-Annexin V scans. Hypoxia enhanced mitochondrial stability, and this was inhibited by 3-BrPA treatment. In particular, HK II levels in permeability transition pore complex immunoprecipitates were reduced after 3-BrPA treatment. In mice treated with 3-BrPA, mean tumor volumes and tumor volume growth were found to be significantly reduced. Moreover, percentages of terminal deoxynucleotidyl transferase–mediated dUTP nick end labeling–positive cells were significantly increased in 3-BrPA–treated mice, and this apoptosis-inducing efficacy was reflected *in vivo* by ^{99m}Tc-hydrazinonicotinamide-Annexin V imaging. Our results show that hypoxia enhances mitochondrial stability via HK II induction and that HK II inhibitor treatment exhibits an *in vivo* antitumor effect by inducing apoptosis. Therefore, HK II inhibitors may be therapeutically useful for the treatment of advanced infiltrative hypovascular HCCs, which are growing in a hypoxic environment. [Mol Cancer Ther 2007;6(9):2554–62]

Introduction

Hepatocellular carcinomas (HCC) commonly originate from chronic liver diseases caused by hepatitis virus infections (1–3). Therefore, HCC surveillance using regular hepatic ultrasonography and serum α-fetoprotein determinations offer a possible means of detecting small HCCs (4–6), which are readily treatable using local ablation therapies (7, 8). Even multinodular or large-sized HCCs, which are not amenable to such local therapies, can be treated by transarterial chemoembolization (9–11). However, HCCs sometimes exhibit an infiltrating rather a mass-forming growth pattern (12). Moreover, this infiltrating type is not readily detected by regular HCC surveillance in patients with chronic liver diseases and usually presents at an advanced stage (13, 14).

Advanced HCCs regardless of type are highly malignant and are characterized by their innate resistance to chemotherapeutic agents that are widely and effectively used in other cancer types (15). Thus, there is an urgent need to develop efficient strategies to treat these cancers. The aggressive growth of advanced infiltrative HCCs may be due to the presence of survival signaling in cancer cells (16). HCCs are characteristically hypervascular tumors (17, 18), which suggests that their growths are associated with neovascularization within growing tumor nodules. However, advanced infiltrative HCCs seldom show hypervascularity, although grow more rapidly than mass-forming types. Therefore, cancer cells in these advanced infiltrative HCCs are likely to generate signals that enable them to survive in hypoxic conditions.

Hexokinase (HK), the first enzyme in a glycolytic pathway, is importantly required to maintain cells under hypoxic conditions (19, 20). Of the four types of HK, HK II is the predominantly overexpressed form in HCCs (21, 22). Therefore, HK II may participate in cancer cell survival in advanced infiltrative HCCs. Indeed, we recently showed that hypoxia stimulates HCC cell growth via HK II induction and that the inhibition of HK II induces apoptotic cell death by activating mitochondrial apoptotic signaling cascades (23).

Mitochondrial membrane permeabilization is a major event in the activation of mitochondrial apoptotic signaling (24, 25), and this permeabilization could be caused by the opening of permeability transition pore complex (PTPC;

Received 2/20/07; revised 6/21/07; accepted 8/2/07.

Grant support: Korean Foundation of Liver Research, Korea Health 21 R&D Project (0412-CR01-0704-0001), and National Cancer Control R&D Program 2003, Ministry of Health and Welfare, Republic of Korea.

The costs of publication of this article were defrayed in part by the payment of page charges. This article must therefore be hereby marked *advertisement* in accordance with 18 U.S.C. Section 1734 solely to indicate this fact.

Requests for reprints: Jung-Hwan Yoon, Seoul National University Hospital, 28 Yungun-dong, Chongno-gu, Seoul 110-744, South Korea. Phone: 82-2-2072-2228; Fax: 82-2-743-6701. E-mail: yoonjh@snu.ac.kr

doi:10.1158/1535-7163.MCT-07-0115

refs. 26, 27). HK II binds to the mitochondrial membrane by interacting with the outer membrane protein voltage-dependent anion channel (VDAC), which controls the rate of release of mitochondrial intermembrane space proteins that activate the apoptotic process. Thus, HK II binding to VDAC may suppress the release of intermembrane space proteins and inhibit apoptosis and thereby contribute to tumor cell survival (28, 29).

In the present study, we hypothesized that the induction of HK II by hypoxia is associated with an enhancement in mitochondrial stability and that thus HK II inhibitors would induce apoptosis in an *in vivo* model of HCC. Collectively, the results of this study show that HK II induction enhances mitochondrial stability and that the inhibition of HK II dissociates this enzyme from PTPC. Moreover, the apoptosis-inducing efficacy of the HK II inhibitor 3-bromopyruvate (3-BrPA) was shown in mice bearing HCCs. Thus, our results suggest that HK II inhibitor may be therapeutically useful for the treatment of advanced HCCs.

Materials and Methods

Chemicals and Reagents

3-BrPA, deoxycholate, trypan blue solution (0.4%), and human Annexin V were purchased from Sigma-Aldrich Chemical Co. Solutions of 3-BrPA were prepared as described previously (30). Annexin V-FITC and propidium iodide were purchased from BD PharMingen. Sodium [2-^{14}C]pyruvate was purchased from Perkin-Elmer Life and Analytical Sciences, Inc.

Cell Culture

Huh-BAT cells (Huh-7 cells stably transfected with a bile acid transporter derived from a well-differentiated HCC, a human HCC cell line; refs. 31, 32) were used for *in vitro* experiments and MH134 cells (a mouse HCC cell line) were used for *in vitro* and *in vivo* experiments. Huh-BAT cells were grown in DMEM supplemented with 10% fetal bovine serum, 100,000 units/L penicillin, and 100 mg/L streptomycin, and MH134 cells were grown in RPMI 1640 supplemented with 10% fetal bovine serum, 100,000 units/L penicillin, and 100 mg/L streptomycin. In all experiments done in this study, cells were serum starved overnight to avoid serum-induced signaling. Depending on the experiment concerned, cells were incubated either under standard culture conditions (20% O_2 and 5% CO_2, at 37°C) or in hypoxic culture conditions (1% O_2, 5% CO_2, and 94% N_2, at 37°C).

Preparation of Mitochondrial and Cytosolic Extracts

Cells were washed twice with PBS, and mitochondrial and cytosolic extracts were isolated using Mitochondria/Cytosol Fractionation kits (BioVision, Inc.) according to the manufacturer's instructions.

Immunoblot Analysis

Cells were lysed for 20 min on ice using lysis buffer [50 mmol/L Tris-HCl (pH 7.4); 1% NP40; 0.25% sodium deoxycholate; 150 mmol/L NaCl; 1 mmol/L EDTA; 1 mmol/L phenylmethylsulfonyl fluoride; 1 μg/mL aprotinin, leupeptin, and pepstatin; 1 mmol/L Na_3VO_4; 1 mmol/L NaF] and centrifuged at 14,000 × *g* for 10 min at 4°C. Samples were resolved by SDS-PAGE, transferred to nitrocellulose membrane, blotted with appropriate primary antibodies, and incubated with peroxidase-conjugated secondary antibodies (Biosource International). Bound antibodies were visualized using a chemiluminescent substrate (enhanced chemiluminescence; Amersham) and exposed to Kodak X-OMAT film. Mouse anti–cytochrome *c* was obtained from BD PharMingen. Goat anti-AIF, goat anti-HK II, and goat anti-actin were obtained from Santa Cruz Biotechnology, Inc. Mouse anti-Smac/DIABLO was obtained from BD Transduction Laboratories.

Immunoprecipitation Analysis

Cell lysates were mixed with 2 μg of antisera to VDAC (Santa Cruz Biotechnology) and incubated overnight at 4°C. Immune complex was immunoprecipitated with 35 μL of Protein A/G PLUS-Agarose (Santa Cruz Biotechnology) and then washed five times for 10 min with 1 mL of washing buffer. Polypeptides were then resolved by boiling with 35 μL of Laemmli sample buffer for 5 min.

Animals

Animal experiments were done with 4-week-old male C3H/He mice (Charles River Laboratories) in accordance with the guidelines established by the Institutional Animal Care and Use Committee of Seoul National University Hospital. Mice were housed under specific pathogen-free conditions. Imaging procedures were carried out under ketamine hydrochloride–induced (80 mg/kg, i.p.) and xylazine hydrochloride–induced (16 mg/kg, i.p.) anesthesia.

Mouse HCC Model

We used an established s.c. HCC mouse model as described previously (33). Briefly, 2.5 × 10^5 viable MH134 cells suspended in 0.1 mL of RPMI 1640 were injected i.d. to produce a bleb in the right flanks of C3H mice. When tumor volumes reached 0.2 cm^3, 3-BrPA was given i.p. for 5 consecutive days. Fourteen days after injecting 3-BrPA, mice were sacrificed by exsanguination via cardiac puncture under general anesthesia (isoflurane inhalation). Tumor masses and liver tissues were then harvested, fixed in 10% formaldehyde, and cryopreserved.

Preparation and Biodistribution of ^{14}C-Labeled BrPA

[2-^{14}C]bromopyruvic acid ([^{14}C]BrPA) was prepared using a modification of the procedure described by Hensel et al. (34). Briefly, 60 μCi of sodium [^{14}C]pyruvate (specific activity, 16.4 μCi/μmol) in 120 μL water were dried by successively adding aliquots acetonitrile under an argon stream at 80°C. Pyruvic acid (83 μL, 1.19 mmol) was then added and the mixture was dissolved in 95 μL chloroform. After adding 61 μL (1.19 mmol) of bromine, the mixture was stirred for 3 h at room temperature and dried for 5 h under an argon stream to provide a pale yellow semisolid. The biodistribution of [^{14}C]BrPA (specific activity, 0.050 μCi/μmol) was evaluated in C3H mice bearing MH134 tumors. Tumor-bearing mice (mean body weight, 23.5 ± 0.4 g) were injected i.v. via a lateral tail vein

with 1 μCi [^{14}C]BrPA, which is equivalent to 3.31 mg BrPA (average BrPA dose, 141 mg/kg). At selected times after injection (1, 2, 4, and 8 h), mice were sacrificed by exsanguination via cardiac puncture under general anesthesia (isoflurane inhalation). Aliquots of heparinized blood were rapidly centrifuged at 2,000 × *g* for 5 min to obtain plasma. Radioactivities of tissues and blood were determined using a β-counter using a liquid scintillation analyzer (Tri-Carb 2300TR, Packard).

Apoptosis

Apoptosis in tumor tissue was investigated by terminal deoxynucleotidyl transferase–mediated dUTP nick end labeling (TUNEL) staining using ApopTag Peroxidase *In situ* Apoptosis Detection kits (Chemicon International) after fixing fresh tissue with 4% paraformaldehyde. Positive TUNEL cells were counted in six different high-power fields at ×400 magnification and averaged. Cell numbers are expressed as percentages of total cells and are referred to as apoptotic indexes.

Cell Viability

Cell viabilities were determined using trypan blue dye exclusion assays. After 4 h of incubation with 3-BrPA, cell pellets were resuspended in PBS. Viable cell numbers were determined by trypan blue staining.

Detection of Apoptosis by Flow Cytometric Analysis

Apoptotic or necrotic cell levels were determined by flow cytometry after double staining with Annexin V-FITC and propidium iodide using an assay kit from BD PharMingen as described previously (35).

2-Fluoro-[^{18}F]-2-Deoxyglucose Uptake and ^{99m}Tc-Hydrazinonicotinamide-Annexin V Binding

2-Fluoro-[^{18}F]-2-deoxyglucose ([^{18}F]FDG) was synthesized by nucleophilic fluorination followed by deprotection using an automated synthesis module as described previously (36). Annexin V was labeled with ^{99m}Tc after derivatization with hydrazinonicotinamide (HYNIC; ref. 37). [^{18}F]FDG (740 kBq; specific activity, 37 GBq/μmol; radiochemical purity, >98%) was then added to each well, and

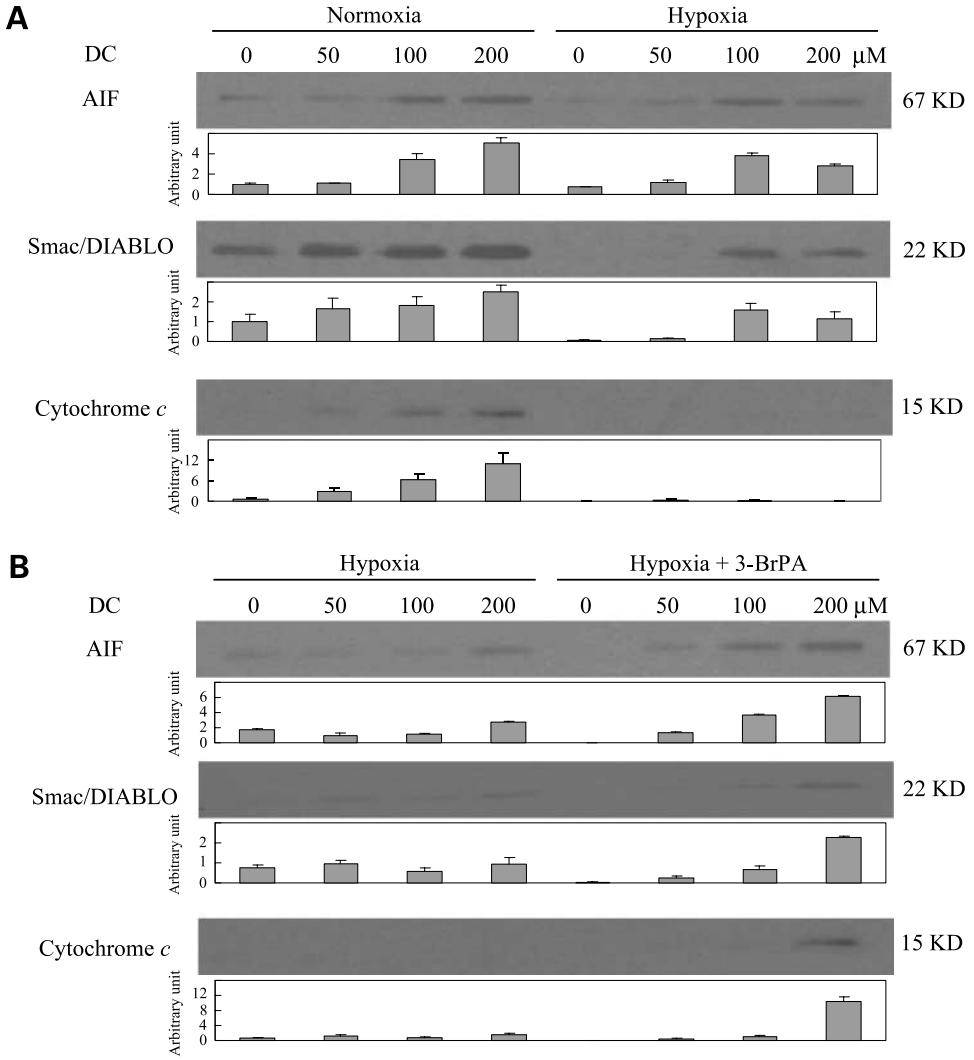

Figure 1. Hypoxia-induced enhancement of mitochondrial stability. **A,** mitochondria were isolated from Huh-BAT cells cultured either in a normoxic or hypoxic state for 36 h. Isolated mitochondria were then incubated in the presence of deoxycholate (*DC*) at 0 to 200 μmol/L for 1 h. Supernatants were then collected and immunoblotting was done for AIF, Smac/DIABLO, and cytochrome *c*. To normalize band intensities, the arbitrary units were calculated by densitometric analysis of intensities of AIF, Smac/DIABLO, and cytochrome *c* bands, assuming that of each control band under normoxic condition at 0 μmol/L deoxycholate as 1. *Columns,* mean of three independent experiments; *bars,* SD. **B,** mitochondria were isolated from Huh-BAT cells cultured in a hypoxic state for 36 h. Isolated mitochondria were then incubated for 1 h with deoxycholate (0–200 μmol/L) in the presence or absence of 3-BrPA (100 μmol/L). Supernatants were then immunoblotted for AIF, Smac/DIABLO, and cytochrome *c*. The arbitrary units were calculated by densitometric analysis of intensities of each band, assuming that of each control band under hypoxic condition at 0 μmol/L deoxycholate as 1. *Columns,* mean of three independent experiments; *bars,* SD.

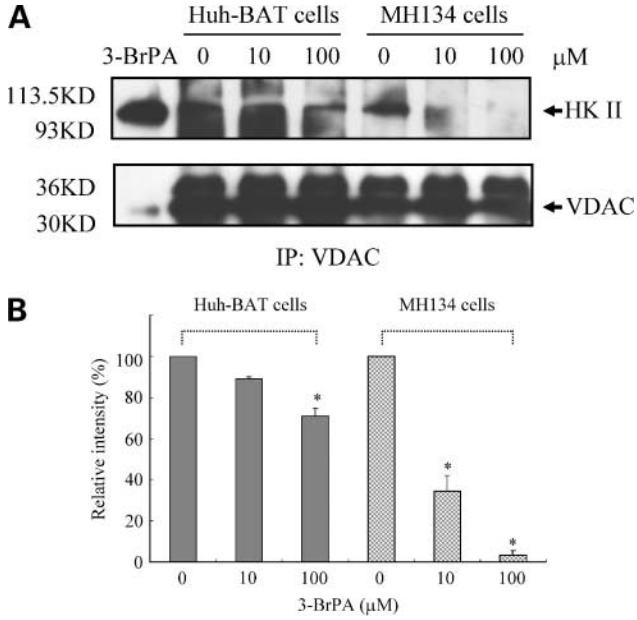

Figure 2. HK II inhibitor-induced compositional alterations of PTPC. **A,** Huh-BAT or MH134 cells were cultured in the presence of 3-BrPA at 0 to 100 μmol/L for 3 h. Mitochondria were isolated, and PTPC was immunoprecipitated using VDAC antibody. Immunoblot analysis was done for HK II and VDAC. **B,** the relative intensities (%) were calculated by densitometric analysis of HK II band intensity relative to VDAC band intensity in the immunoprecipitate, assuming that of each control (3-BrPA, 0 μmol/L) as 100%. *Columns,* mean of three independent experiments; *bars,* SD. *, $P < 0.05$ versus control.

after a 60-min incubation period, the medium was removed and cells were washed twice with ice-cold PBS. After 4 h of incubation with 3-BrPA, cells were collected, washed with cold PBS, and suspended in Annexin V–binding buffer in test tubes. ^{99m}Tc-HYNIC-Annexin V (74 kBq; specific activity, 370–740 MBq or 10–20 μCi/μg protein; radiochemical purity, >98%) was then added to each tube. After a 30-min incubation period, the buffer was removed and cells were washed twice with ice-cold PBS. Cell pellets were then counted using a well-type gamma counter (1480 WIZARD, Wallac Oy). The accumulations of [^{18}F]FDG and ^{99m}Tc-HYNIC-Annexin V in cells were expressed as percentage activity versus injected dose (%ID).

^{99m}Tc-HYNIC-Annexin V Scan

^{99m}Tc-HYNIC-Annexin V (50 μCi) was injected via a tail vein 1 and 3 days after 3-BrPA treatment. Planar scans were acquired 1 h after injecting ^{99m}Tc-HYNIC-Annexin V using a gamma camera.

Statistical Analysis

All data represent at least three independent experiments using cells from a minimum of three separate isolations and are expressed as mean ± SD. Statistical evaluations of numerical variables in three 3-BrPA dosage groups were conducted using the Mann-Whitney *U* test and the Kruskal-Wallis test. Differences in tumor growth were statistically analyzed using repeated measures ANOVA. A scattergram of Annexin V–positive cell fraction and ^{99m}Tc-HYNIC-Annexin V uptake was plotted using linear regression analysis (Spearman correlation test). All statistical analyses were done using Statistical Package for the Social Sciences 12.0 for Windows (SPSS, Inc.). *P* values of <0.05 were considered statistically significant.

Results

Hypoxia Enhances Mitochondrial Stability

Mitochondria were isolated from Huh-BAT cells cultured in normoxic or hypoxic states. Isolated mitochondria were then incubated in the presence of deoxycholate, which is known to enhance mitochondrial membrane permeabilization (38). Mitochondria isolated from cells cultured in a hypoxic state were more resistant to the permeability-enhancing effect of deoxycholate than those from cells

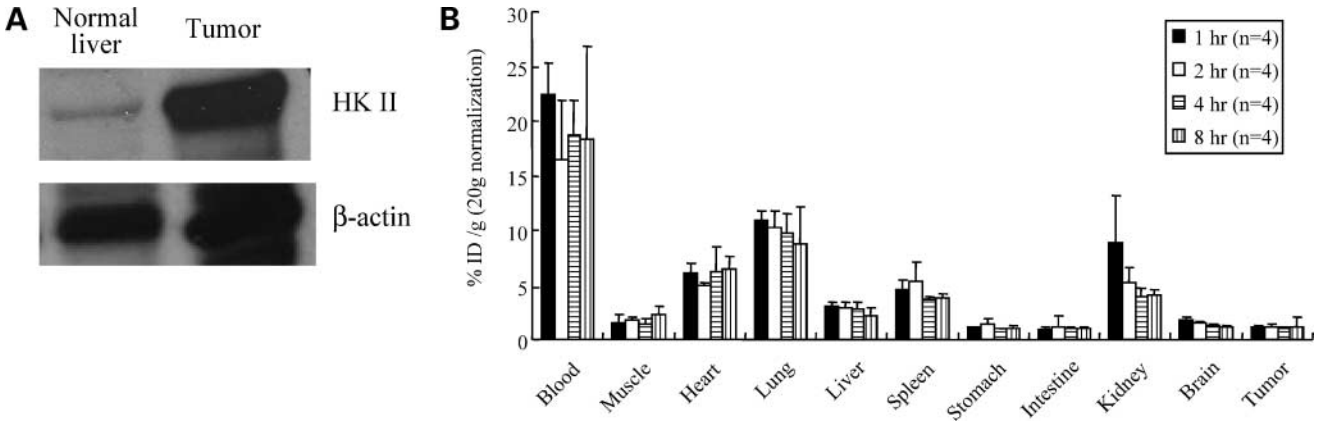

Figure 3. HK II overexpression and biodistribution of ^{14}C-labeled BrPA in mice bearing an MH134 tumor. **A,** an animal model of HCC in C3H mice was established by the i.d. implantation of MH134 cells. Tumor and liver tissues were harvested, and equivalent amounts of proteins were immunoblotted with anti-HK II and anti-actin antibody. **B,** tumor-bearing mice were injected i.v. via the lateral tail vein with 4 μCi/0.1 mL of [^{14}C]BrPA. At the indicated times after injection, radioactivity in tissues or blood was determined using a β-counter. Results are expressed as dose per gram of tissue as a percentage of injected radioactivity (%IDg^{-1}). Four mice were used at each time point. *Columns,* mean values of the treated groups; *bars,* SD.

cultured under normoxic conditions (Fig. 1A). Moreover, when isolated mitochondria from hypoxic cells were simultaneously incubated with deoxycholate and 3-BrPA, cytochrome *c* release occurred at a lower deoxycholate concentration than for mitochondria treated with deoxycholate alone (Fig. 1B). These findings indicate that hypoxia enhances mitochondrial stability and that the HK II inhibitor 3-BrPA attenuates this enhancement.

Compositional Alterations in PTPC Induced by HK II Inhibitor

Because PTPC regulates mitochondrial stability and HK II is a major component of PTPC, we hypothesized that 3-BrPA may induce the dissociation of HK II from PTPC to open PTPC and thus allow the release of cytochrome *c* into the cytosol. To test this hypothesis, PTPC was immunoprecipitated using antisera for VDAC from the mitochondrial fractions of Huh-BAT or MH134 cells, which were cultured in the presence of 3-BrPA at 0 to 100 μmol/L. HK II was identified in PTPC immunoprecipitates, as shown in Fig. 2A, and this band intensity diminished in a dose-dependent manner when cells were treated in the presence of 3-BrPA (Fig. 2B). Thus, these findings suggest that hypoxia enhances mitochondrial stability by inducing HK II association with PTPC and that 3-BrPA dissociates HK II from and thus activates mitochondrial apoptotic signals.

Antitumor Efficacy of 3-BrPA in an *In vivo* Model of HCC

To evaluate antitumor efficacy of 3-BrPA in an *in vivo* model of HCC, we established an animal model of HCC in C3H mice by i.d. implanting MH134 cells. We first verified that our mouse model represented a HK II–overexpressing HCC model, and as shown in Fig. 3A, mouse HCC tumors overexpressed HK II versus normal liver tissues.

We next examined the biodistribution and the stability of [^{14}C]BrPA in MH134-bearing C3H mice. As shown in Fig. 3B, [^{14}C]BrPA distributed into all tissues. In particular, its radioactivity profiles in all tissues showed rapid uptake and delayed washout. Overall, highest radioactivity was observed in blood, kidneys, and lungs. In particular, the blood radioactivity of [^{14}C]BrPA was maintained at a high level throughout the 8-h observation period.

Tumor-bearing mice were then treated with 3-BrPA (0, 5, and 10 mg/kg, i.p. daily for 5 days). The antitumor efficacy of 3-BrPA was first evaluated by measuring tumor volumes. MH134 cells effectively produced tumors in control mice within 14 days of i.d. injection. However, tumor volumes in 3-BrPA–treated mice were significantly reduced compared with the control mice in a dose-dependent manner (mean tumor volume, 1.07 versus 0.58 versus 0.39 cm^3 in 3-BrPA at 0, 5, and 10 mg/kg, respectively; $P = 0.047$; Fig. 4A). To control for variations in initial tumor volume in individual mice, we also compared tumor growth rates by dividing differences between posttreatment (day 14) and pretreatment tumor volumes (day 0) by pretreatment volumes. In control mice, tumor volumes increased 4- to 9-fold, whereas this was significantly reduced in 3-BrPA–treated mice (Fig. 4B). These observations suggest that HK II inhibitor treatment exhibits *in vivo* antitumor efficacy.

In vivo Demonstration of the Apoptosis-Inducing Efficacy of 3-BrPA

We next evaluated whether 3-BrPA induces apoptosis in mouse HCC tumors. To quantify apoptosis in tumors, we first used TUNEL staining. Percentages of TUNEL-stained cells were significantly higher in 3-BrPA–treated mice (0.53 versus 1.40 versus 1.84% for mice treated with 3-BrPA at 0, 5, and 10 mg/kg, respectively; $P = 0.018$; Fig. 5A and B).

We also confirmed the apoptosis-inducing efficacy of 3-BrPA using ^{99m}Tc-HYNIC-Annexin V scans. The validity of the method used was first evaluated *in vitro*. Briefly, MH134 cells were cultured in the presence of 3-BrPA

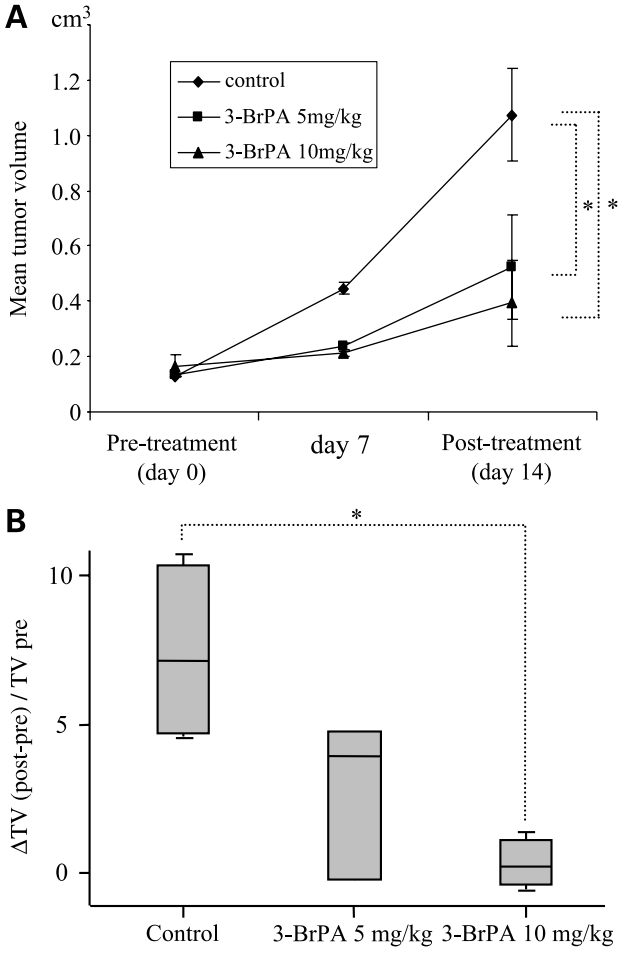

Figure 4. *In vivo* antitumor efficacy of the HK II inhibitor 3-BrPA. In mice bearing an MH134 tumor, 3-BrPA was given (0, 5, and 10 mg/kg, daily i.p. for 5 d). **A,** tumor volumes were calculated by measuring tumor lengths (L) and widths (W) of sagittal sections and calculated using 0.5 × L (cm) × W^2 (cm^2). Four mice were randomly allocated into each of these 3-BrPA dosage groups. *Points,* mean tumor volumes; *bars,* SE. *, $P < 0.05$ versus control. **B,** tumor growth rates were calculated by dividing differences between posttreatment (day 14) and pretreatment tumor volumes (*TV*; day 0) by pretreatment volumes. *Columns,* mean values of the three 3-BrPA dosage groups; *bars,* SD. *, $P < 0.05$ versus control.

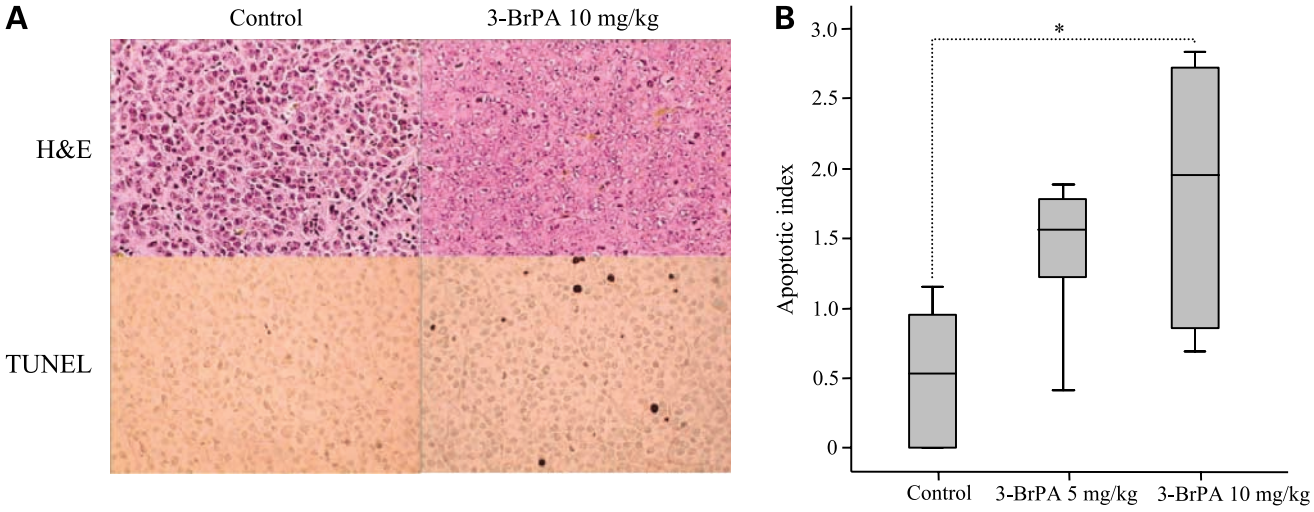

Figure 5. *In vivo* demonstration of the apoptosis-inducing efficacy of 3-BrPA by TUNEL staining. **A,** H&E and TUNEL staining of tumor tissues in control and 3-BrPA–treated mice. Original magnification, ×400. **B,** TUNEL-positive cell percentages (apoptotic indexes) were determined in six different high-power (×400 magnification) fields. *Columns,* mean values of the three 3-BrPA dosage groups; *bars,* SD. *, $P < 0.05$ versus control.

(0–100 μmol/L), and cell viabilities were measured using trypan blue dye exclusion assays. 3-BrPA (0, 25, 50, and 100 μmol/L) was found to reduce viability in a dose-dependent manner (Fig. 6A). Moreover, these viability reductions were found to be well correlated with apoptotic cell fractions, determined as Annexin V-FITC–positive fractions by flow cytometry (Fig. 6A and B). Moreover, apoptotic cell fractions were positively correlated with ^{99m}Tc-HYNIC-Annexin V uptake (%ID) in a 3-BrPA dose-dependent manner ($\gamma^2 = 0.698$; $P < 0.05$; Fig. 6C). In contrast, a significant decrease in [^{18}F]FDG uptake (%ID) was observed even in cells treated with the lowest concentration of 3-BrPA (25 μmol/L; $P < 0.01$), and no additional changes in [^{18}F]FDG uptake (%ID) were observed at 3-BrPA concentrations higher than 25 μmol/L (Fig. 6A). These findings indicate that ^{99m}Tc-HYNIC-Annexin V uptake following 3-BrPA treatment sensitively quantifies cellular apoptosis. Indeed, in tumor-bearing mice, ^{99m}Tc-HYNIC-Annexin V imaging showed tumor-to-background uptake ratios of 1.92 at 1 day and 4.23 at 3 days after 5 mg/kg of 3-BrPA treatment (nontreated tumors had a mean uptake ratio of 2.93; Fig. 6D). These findings indicate that 3-BrPA induces apoptosis in an *in vivo* model of HCC and that this apoptosis-inducing efficacy is reflected *in vivo* by ^{99m}Tc-HYNIC-Annexin V imaging.

Discussion

The key findings of the present study relate to the participation of HK II in the regulation of mitochondrial stability in HCC cells. In particular, this study shows that hypoxia enhances mitochondrial stability via HK II induction and that HK II inhibition activates mitochondrial apoptotic signals. Moreover, the systemically given HK II inhibitor exhibited antitumor efficacy by inducing apoptosis.

We have previously reported that hypoxia induces HK II expression in HCC cells (23). In the present study, we also show that hypoxia-mediated HK II induction enhances mitochondrial stability and that 3-BrPA induces structural alteration in PTPC, which leads to the activation of mitochondrial apoptotic signaling. The mechanisms underlying activation of mitochondrial apoptotic signaling are complex and multiple mechanisms result in cytochrome *c* release. For example, proapoptotic Bcl2 family proteins, such as *t*Bid, Bax/Bak, and Bim, regulate apoptosis by interacting with VDAC in the mitochondrial outer membrane (28, 39, 40). It is also possible that the opening of mitochondrial permeability transition pores (41) is involved in the outer membrane rupture that allows the release of intermembrane proteins such as cytochrome *c*, AIF, and Smac/DIABLO (42, 43). Although the structure of mitochondrial permeability transition pore has not been completely elucidated, PTPC is a complex composed of a variety of proteins, which include VDAC, ANT, CypD, and HK II (44–47). The present study shows that the HK II inhibitor 3-BrPA causes the dissociation of HK II from PTPC and that this causes PTPC opening and the release of cytochrome *c* into the cytosol. Therefore, these observations collectively suggest that HK II induction is one of the major mechanisms of cell survival in hypoxic environments, such as that in advanced infiltrative hypovascular HCCs, and that HK II inhibitors may exhibit antitumor efficacy by activating mitochondrial apoptotic signals in these advanced tumors.

We also evaluated the *in vivo* antitumor efficacy of 3-BrPA. Several *in vivo* studies using rat AS-30D or rabbit VX2 HCC models have shown the antitumor efficacy of 3-BrPA (30, 48). However, these studies evaluated the

efficacy of locally injected 3-BrPA via selective intraarterial or intratumoral injection, whereas the present study shows the antitumor efficacy of i.p. given 3-BrPA. I.p. administration is a means of systemic delivery, as it allows peritoneal absorption and subsequent portal delivery, which mimics the effects of oral administration. Moreover, we also evaluated the antitumor efficacy of 3-BrPA *in vivo* by quantifying apoptosis and measuring tumor volumes. As shown by our TUNEL staining findings, apoptotic cells were significantly more abundant in 3-BrPA–treated mice than in nontreated controls. However, the TUNEL staining method used is only applicable in retrieved tumor tissues, and therefore, we also attempted to evaluate the apoptosis-inducing efficacy

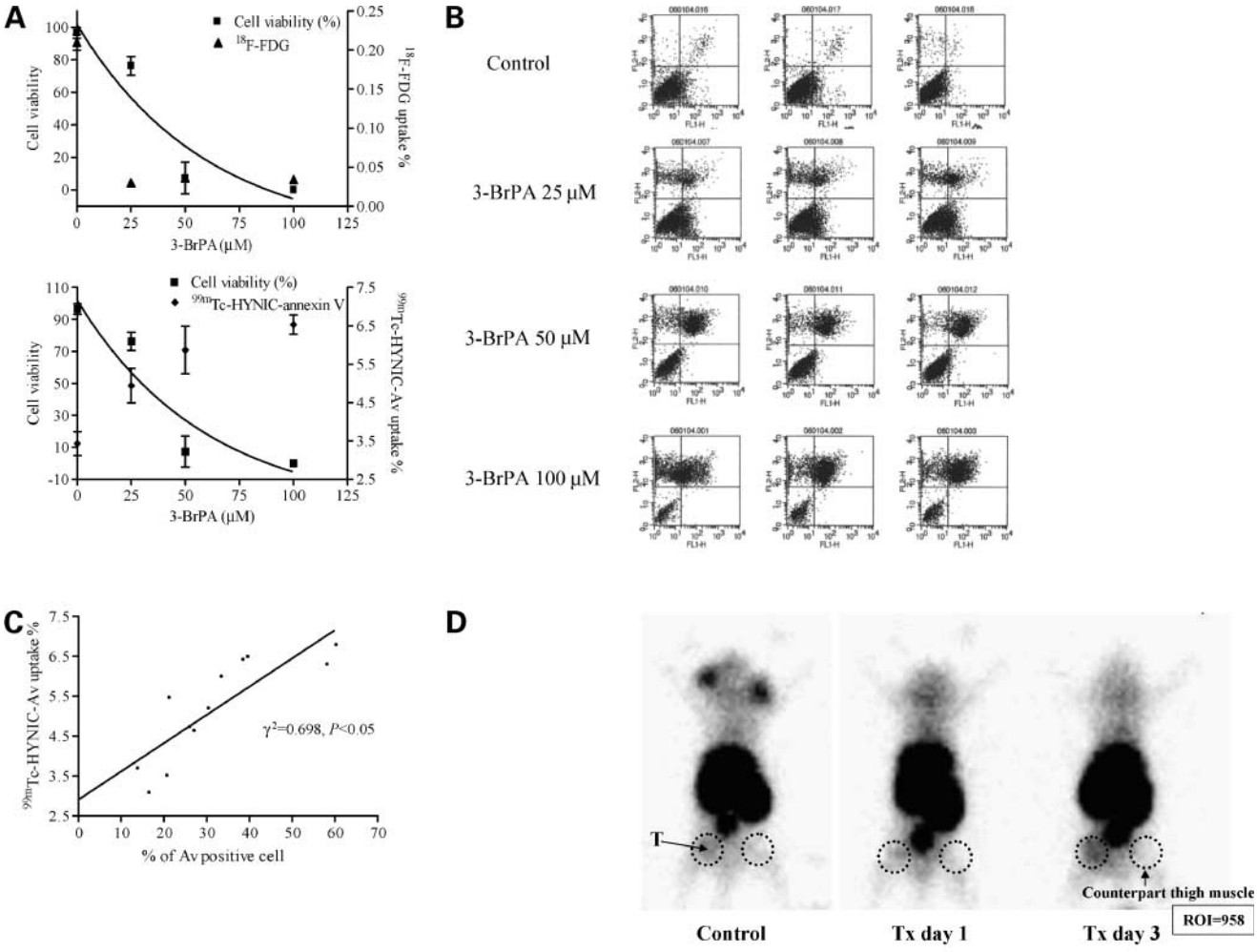

	Control	Treatment (day 1)	Treatment (day 3)
Tumor Volume (cm^3)	0.12	0.091	0.24
Region-of-Interest (ROI) Count	2356	1835	4055

Figure 6. Validity of ^{99m}Tc-HYNIC-Annexin V uptake for measuring apoptosis and ^{99m}Tc-HYNIC-Annexin V imaging. **A,** MH134 cells were treated with 3-BrPA for 4 h. Cell viabilities (% of control, ■) were assessed by trypan blue exclusion. [^{18}F]FDG uptake (%, ▲) was determined 1 h after adding [^{18}F]FDG (740 kBq). *In vitro* binding (%, ♦) of ^{99m}Tc-HYNIC-Annexin V (*Av*) was examined 30 min after adding ^{99m}Tc-HYNIC-Annexin V (37 kBq). *Points,* mean of three independent experiments; *bars,* SD. **B,** cell death was measured by the flow cytometric analysis of cells double stained with Annexin V (*X axis*) and propidium iodide (*Y axis*). Values presented represent three independent experiments. **C,** correlation between the Annexin V – positive cell fraction by flow cytometry and the ^{99m}Tc-HYNIC-Annexin V uptake rate (expressed as percentage of injected radioactivity; %ID). Individual data points are plotted in the scattergram and the regression line shows a linear correlation between the two. **D,** in mice bearing an MH134 tumor, 3-BrPA was given i.p. (5 mg/kg, daily for 5 d). ^{99m}Tc-HYNIC-Annexin V (50 μCi/2 μg/0.1 mL/head) was injected into a tail vein. Gamma camera images were obtained 1 h later. *T,* tumor (MH134 tumor).

of systemically given 3-BrPA using ^{99m}Tc-labeled Annexin V *in vivo* imaging (49). The validity of this imaging modality was confirmed by our *in vitro* experiments, which showed ^{99m}Tc-HYNIC-Annexin V uptake in apoptotic mouse HCC cells. Moreover, this imaging modality was also able to dynamically quantify cellular apoptosis following 3-BrPA injection even before tumor regression. In contrast, [^{18}F]FDG scans were unsuitable for monitoring the *in vivo* antitumor efficacy of 3-BrPA because HK II inhibitor suppressed [^{18}F]FDG uptake as well as glucose uptake in cells treated with even the lowest concentration of 3-BrPA (25 μmol/L). Therefore, these findings collectively indicate that systemically given 3-BrPA may exhibit antitumor efficacy by inducing cellular apoptosis and that this may be quantifiable by ^{99m}Tc-labeled Annexin V *in vivo* imaging.

Human HCC cells overexpress HK II, as we showed previously (23). Moreover, in the present study, we also observed HK II overexpression in tumor tissues compared with normal liver tissues (Fig. 3A), and thus, 3-BrPA uptake by normal liver tissues is expected to be negligible. Indeed, the distribution of [^{14}C]BrPA in liver was low in the present study. Moreover, no adverse effect or toxicity was found following 3-BrPA administration, and no significant difference in mean body weights was observed among mice treated with different doses of 3-BrPA or between these and control mice (data not shown). In addition, in liver tissue blocks obtained from 3-BrPA–treated mice, no pathologic features or increases in hepatocyte apoptotic indices were observed versus control mice (data not shown). Therefore, these findings collectively suggest that 3-BrPA treatment might be a selective anticancer therapy because its uptake in HCC cells is maximized by high HK II expression levels, whereas its uptake by surrounding normal liver tissue is minimized.

In conclusion, the present study shows that hypoxia enhances mitochondrial stability via HK II induction and that the inhibition of HK II causes release of this enzyme from PTPC, thus leading to the activation of mitochondrial apoptotic signals. Moreover, the apoptosis-inducing efficacy of HK II inhibitor was shown in animals bearing HCCs. Therefore, we conclude that blockage of HK II may be therapeutically useful for the management of advanced infiltrative hypovascular HCCs, which are aggressively growing in a relatively hypoxic environment.

References

1. Liang TJ, Jeffers LJ, Reddy KR, et al. Viral pathogenesis of hepatocellular carcinoma in the United States. Hepatology 1993;18:1326 – 33.

2. Colombo M, de Franchis R, Del Ninno E, et al. Hepatocellular carcinoma in Italian patients with cirrhosis. N Engl J Med 1991;325:675 – 80.

3. Koike K. Role of hepatitis viruses in multistep hepatocarcinogenesis. Dig Liver Dis 2001;33:2 – 6.

4. Collier J, Sherman M. Screening for hepatocellular carcinoma. Hepatology 1998;27:273 – 8.

5. Bottelli R, Tibballs J, Hochhauser D, Watkinson A, Dick R, Burroughs AK. Ultrasound screening for hepatocellular carcinoma (HCC) in cirrhosis: the evidence for an established clinical practice. Clin Radiol 1998;53:713 – 6.

6. Cedrone A, Covino M, Caturelli E, et al. Utility of α-fetoprotein (AFP) in the screening of patients with virus-related chronic liver disease: does different viral etiology influence AFP levels in HCC? A study in 350 western patients. Hepatogastroenterology 2000;47:1654 – 8.

7. Shiina S, Teratani T, Obi S, Hamamura K, Koike Y, Omata M. Nonsurgical treatment of hepatocellular carcinoma: from percutaneous ethanol injection therapy and percutaneous microwave coagulation therapy to radiofrequency ablation. Oncology 2002;62 Suppl 1:64 – 8.

8. Yuen MF, Cheng CC, Lauder IJ, Lam SK, Ooi CG, Lai CL. Early detection of hepatocellular carcinoma increases the chance of treatment: Hong Kong experience. Hepatology 2000;31:330 – 5.

9. Llovet JM, Real MI, Montana X, et al. Arterial embolisation or chemoembolisation versus symptomatic treatment in patients with unresectable hepatocellular carcinoma: a randomised controlled trial. Lancet 2002;359:1734 – 9.

10. Lo CM, Ngan H, Tso WK, et al. Randomized controlled trial of transarterial lipiodol chemoembolization for unresectable hepatocellular carcinoma. Hepatology 2002;35:1164 – 71.

11. Bruix J, Sala M, Llovet JM. Chemoembolization for hepatocellular carcinoma. Gastroenterology 2004;127:S179 – 88.

12. Trevisani F, Caraceni P, Bernardi M, et al. Gross pathologic types of hepatocellular carcinoma in Italian patients. Relationship with demographic, environmental, and clinical factors. Cancer 1993;72:1557 – 63.

13. Kanematsu M, Semelka RC, Leonardou P, Mastropasqua M, Lee JK. Hepatocellular carcinoma of diffuse type: MR imaging findings and clinical manifestations. J Magn Reson Imaging 2003;18:189 – 95.

14. Sawabe M, Nakamura T, Kanno J, Kasuga T. Analysis of morphological factors of hepatocellular carcinoma in 98 autopsy cases with respect to pulmonary metastasis. Acta Pathol Jpn 1987;37:1389 – 404.

15. Matsunaga T, Shirasawa H, Hishiki T, et al. Expression of MRP and cMOAT in childhood neuroblastomas and malignant liver tumors and its relevance to clinical behavior. Jpn J Cancer Res 1998;89:1276 – 83.

16. Weinstein-Oppenheimer CR, Henriquez-Roldan CF, Davis JM, et al. Role of the Raf signal transduction cascade in the *in vitro* resistance to the anticancer drug doxorubicin. Clin Cancer Res 2001;7:2898 – 907.

17. Ng IO, Poon RT, Lee JM, Fan ST, Ng M, Tso WK. Microvessel density, vascular endothelial growth factor and its receptors Flt-1 and Flk-1/KDR in hepatocellular carcinoma. Am J Clin Pathol 2001;116:838 – 45.

18. Dupuy E, Hainaud P, Villemain A, et al. Tumoral angiogenesis and tissue factor expression during hepatocellular carcinoma progression in a transgenic mouse model. J Hepatol 2003;38:793 – 802.

19. Bustamante E, Pedersen PL. High aerobic glycolysis of rat hepatoma cells in culture: role of mitochondrial hexokinase. Proc Natl Acad Sci U S A 1977;74:3735 – 9.

20. Bustamante E, Morris HP, Pedersen PL. Energy metabolism of tumor cells. Requirement for a form of hexokinase with a propensity for mitochondrial binding. J Biol Chem 1981;256:8699 – 704.

21. Nakashima RA, Paggi MG, Scott LJ, Pedersen PL. Purification and characterization of a bindable form of mitochondrial bound hexokinase from the highly glycolytic AS-30D rat hepatoma cell line. Cancer Res 1988;48:913 – 9.

22. Mathupala SP, Rempel A, Pedersen PL. Glucose catabolism in cancer cells. Isolation, sequence, and activity of the promoter for type II hexokinase. J Biol Chem 1995;270:16918 – 25.

23. Gwak GY, Yoon JH, Kim KM, Lee HS, Chung JW, Gores GJ. Hypoxia stimulates proliferation of human hepatoma cells through the induction of hexokinase II expression. J Hepatol 2005;42:358 – 64.

24. Costantini P, Jacotot E, Decaudin D, Kroemer G. Mitochondrion as a novel target of anticancer chemotherapy. J Natl Cancer Inst 2000;92:1042 – 53.

25. Kroemer G, Reed JC. Mitochondrial control of cell death. Nat Med 2000;6:513 – 9.

26. Marzo I, Brenner C, Zamzami N, et al. Bax and adenine nucleotide translocator cooperate in the mitochondrial control of apoptosis. Science 1998;281:2027 – 31.

27. Brenner C, Cadiou H, Vieira HL, et al. Bcl-2 and Bax regulate the channel activity of the mitochondrial adenine nucleotide translocator. Oncogene 2000;19:329 – 36.

28. Pastorino JG, Shulga N, Hoek JB. Mitochondrial binding of hexokinase II inhibits Bax-induced cytochrome *c* release and apoptosis. J Biol Chem 2002;277:7610 – 8.

29. Pastorino JG, Hoek JB. Hexokinase II: the integration of energy metabolism and control of apoptosis. Curr Med Chem 2003;10:1535 – 51.

30. Ko YH, Smith BL, Wang Y, et al. Advanced cancers: eradication in all cases using 3-bromopyruvate therapy to deplete ATP. Biochem Biophys Res Commun 2004;324:269 – 75.

31. Higuchi H, Bronk SF, Takikawa Y, et al. The bile acid glycochenodeoxycholate induces trail-receptor 2/DR5 expression and apoptosis. J Biol Chem 2001;276:38610 – 8.

32. Nakabayashi H, Taketa K, Miyano K, Yamane T, Sato J. Growth of human hepatoma cells lines with differentiated functions in chemically defined medium. Cancer Res 1982;42:3858 – 63.

33. Yamashita YI, Shimada M, Hasegawa H, et al. Electroporation-mediated interleukin-12 gene therapy for hepatocellular carcinoma in the mice model. Cancer Res 2001;61:1005 – 12.

34. Hensel R, Mayr U, Woenckhaus C. Affinity labelling of the allosteric site of the L-lactate dehydrogenase of *Lactobacillus casei*. Eur J Biochem 1983;135:359 – 65.

35. Xu RH, Pelicano H, Zhou Y, et al. Inhibition of glycolysis in cancer cells: a novel strategy to overcome drug resistance associated with mitochondrial respiratory defect and hypoxia. Cancer Res 2005;65:613 – 21.

36. Hamacher K, Coenen HH, Stocklin G. Efficient stereospecific synthesis of no-carrier-added 2-[^{18}F]-fluoro-2-deoxy-D-glucose using aminopolyether supported nucleophilic substitution. J Nucl Med 1986; 27:235 – 8.

37. Blankenberg FG, Katsikis PD, Tait JF, et al. *In vivo* detection and imaging of phosphatidylserine expression during programmed cell death. Proc Natl Acad Sci U S A 1998;95:6349 – 54.

38. Botla R, Spivey JR, Aguilar H, Bronk SF, Gores GJ. Ursodeoxycholate (UDCA) inhibits the mitochondrial membrane permeability transition induced by glycochenodeoxycholate: a mechanism of UDCA cytoprotection. J Pharmacol Exp Ther 1995;272:930 – 8.

39. Wei MC, Zong WX, Cheng EH, et al. Proapoptotic BAX and BAK: a requisite gateway to mitochondrial dysfunction and death. Science 2001; 292:727 – 30.

40. Pastorino JG, Hoek JB, Shulga N. Activation of glycogen synthase kinase 3β disrupts the binding of hexokinase II to mitochondria by phosphorylating voltage-dependent anion channel and potentiates chemotherapy-induced cytotoxicity. Cancer Res 2005;65:10545 – 54.

41. Crompton M, Ellinger H, Costi A. Inhibition by cyclosporin A of a Ca^{2+}-dependent pore in heart mitochondria activated by inorganic phosphate and oxidative stress. Biochem J 1988;255:357 – 60.

42. Bradham CA, Qian T, Streetz K, Trautwein C, Brenner DA, Lemasters JJ. The mitochondrial permeability transition is required for tumor necrosis factor α-mediated apoptosis and cytochrome *c* release. Mol Cell Biol 1998; 18:6353 – 64.

43. Hatano E, Bradham CA, Stark A, Iimuro Y, Lemasters JJ, Brenner DA. The mitochondrial permeability transition augments Fas-induced apoptosis in mouse hepatocytes. J Biol Chem 2000;275:11814 – 23.

44. Marzo I, Brenner C, Zamzami N, et al. The permeability transition pore complex: a target for apoptosis regulation by caspases and bcl-2-related proteins. J Exp Med 1998;187:1261 – 71.

45. Belzacq AS, Vieira HL, Kroemer G, Brenner C. The adenine nucleotide translocator in apoptosis. Biochimie 2002;84:167 – 76.

46. Zoratti M, Szabo I. The mitochondrial permeability transition. Biochim Biophys Acta 1995;1241:139 – 76.

47. O'Gorman E, Beutner G, Dolder M, Koretsky AP, Brdiczka D, Wallimann T. The role of creatine kinase in inhibition of mitochondrial permeability transition. FEBS Lett 1997;414:253 – 7.

48. Geschwind JF, Ko YH, Torbenson MS, Magee C, Pedersen PL. Novel therapy for liver cancer: direct intraarterial injection of a potent inhibitor of ATP production. Cancer Res 2002;62:3909 – 13.

49. Belhocine TZ, Blankenberg FG. ^{99m}Tc-Annexin A5 uptake and imaging to monitor chemosensitivity. Methods Mol Med 2005;111: 363 – 80.